MRI of Retinal Free Radical Production With Laminar Resolution In Vivo

Bruce A. Berkowitz,[1,2] Alfred S. Lewin,[3] Manas R. Biswal,[3] Bryce X. Bredell,[1] Christopher Davis,[1] and Robin Roberts[1]

[1]Department of Anatomy and Cell Biology, Wayne State University School of Medicine, Detroit, Michigan, United States
[2]Department of Ophthalmology, Wayne State University School of Medicine, Detroit, Michigan, United States
[3]Department of Molecular Genetics and Microbiology, University of Florida, Gainesville, Florida, United States

Correspondence: Bruce A. Berkowitz, Wayne State University School of Medicine, 540 E. Canfield, Detroit, MI 48201, USA; baberko@med.wayne.edu.

BXB and CD contributed equally to the work presented here and should therefore be regarded as equivalent authors.

Submitted: December 17, 2015
Accepted: January 15, 2016

Citation: Berkowitz BA, Lewin AS, Biswal MR, Bredell BX, Davis C, Roberts R. MRI of retinal free radical production with laminar resolution in vivo. *Invest Ophthalmol Vis Sci*. 2016;57:577–585. DOI:10.1167/iovs.15-18972

Purpose. Recent studies have suggested the hypothesis that quench-assisted 1/T1 magnetic resonance imaging (MRI) measures free radical production with laminar resolution in vivo without the need of a contrast agent. Here, we test this hypothesis further by examining the spatial and detection sensitivity of quench-assisted 1/T1 MRI to strain, age, or retinal cell layer-specific genetic manipulations.

Methods. We studied: adult wild-type mice; mice at postnatal day 7 (P7); cre dependent retinal pigment epithelium (RPE)-specific MnSOD knockout mice; doxycycline-treated *Sod2*$^{flox/flox}$ mice lacking the cre transgene; and α-transducin knockout (*Gnat1*$^{-/-}$) mice on a C57Bl/6 background. Transretinal 1/T1 profiles were mapped in vivo in the dark without or with antioxidant treatment, or followed by light exposure. We calibrated profiles spatially using optical coherence tomography.

Results. Dark-adapted RPE-specific MnSOD knockout mice had greater than normal 1/T1 in the RPE and outer nuclear layers that was corrected to wild-type levels by antioxidant treatment. Dark and light *Gnat1*$^{-/-}$ mice also had greater than normal outer retinal 1/T1 values. In adult wild-type mice, dark values of 1/T1 in the ellipsoid region and in the outer segment were suppressed by 13 minutes of light. By 29 minutes of light, 1/T1 reduction extended to the outer nuclear layer. *Gnat1*$^{-/-}$ mice demonstrated a faster light-evoked suppression of 1/T1 values in the outer retina. In P7 mice, transretinal 1/T1 profiles were the same in dark and light.

Conclusions. Quench-assisted MRI has the laminar resolution and detection sensitivity to evaluate normal and pathologic production of free radicals in vivo.

Keywords: oxidative stress, rods, MRI, free radicals, retina

Rod cell oxidative stress, the continual generation of free radicals exceeding a cell's quenching capacity, has been implicated in the pathogenesis of currently untreatable, degenerative diseases of the retina, including retinitis pigmentosa and diabetic retinopathy.[1–16] However, clinical benefits from antioxidant treatment have not been realized, perhaps because a one-size-fits-all approach may be too simple and also because we cannot assess antioxidant treatment efficacy in vivo on rod cells. Conventional methods, such as optical coherence tomography (OCT) and electrophysiology (ERG), do not measure rod cell free radical production. Recent methods have examined redox-responsive probes to evaluate oxidative stress from specific reactive oxygen species in vivo, but these approaches are problematic because they (1) modify the redox environment by the presence of the reporter probes, (2) require careful consideration of the biologic time course of the probe, (3) require intravitreal injections, and (4) measure fundus oxidative stress without laminar resolution.[17–20] Thus, the use of these methods for longitudinal studies and in the clinic is unlikely, limiting objective evaluation of antioxidant treatment efficacy over time within rod cells.

Recently, we, and others, unmasked a contribution of continuously produced free radicals to the spin-lattice relaxation rate (1/T1) magnetic resonance imaging (MRI) signal by collecting data in the absence and presence of a quenching condition ("quench-assisted MRI").[21,22] Quench-assisted 1/T1 MRI measured outer retina oxidative stress following pharmacological manipulation.[21] Furthermore, quench-assisted MRI reliably reported the in vivo suppression of free radical production in healthy outer retina in response to a light quench.[21] For example, light quench-assisted MRI readily distinguished between the expected differences in the light response of rods of 129S6 wild-type mice versus cones of *R91W;Nrl*$^{-/-}$ mice.[21] These results suggest that light-evoked suppression of outer retinal 1/T1 signal is linked with reduced leakage of free radicals from mitochondria.[9,23]

Here, we extend the above studies by testing the spatial and detection sensitivity of quench-assisted MRI to strain, age, or retinal cell layer-specific genetic manipulations. The following groups were evaluated: (1) a common wild-type mouse strain, the C57Bl/6 mouse, (2) immature mice before outer retinal photosensitivity develops, postnatal day 7 mice (P7), (3) mutant mice missing mitochondrial superoxide dismutase (SOD) from only the retinal pigment epithelium (RPE) layer (and their controls), and (4) mice lacking rod specific α-transducin (*Gnat1*). α-transducin is an essential signaling

element for rod phototransduction.[24,25] In general, because *Gnat1*$^{-/-}$ mice have inoperant rod phototransduction without retinal degeneration, they allow for the exploration of cone responses to light, as well as rhodopsin regeneration via the visual cycle.[26,27] In this study, quench-assisted MRI outcomes in vivo in these groups matched results generated from previous studies using ex vivo methods. Overall, our results provide further support for the hypothesis that quench-assisted MRI has the cellular and subcellular spatial resolution, and detection sensitivity, for evaluating normal and pathologic production of retinal free radical production in vivo.

Materials and Methods

All animals were treated in accordance with the National Institutes of Health Guide for the Care and Use of Laboratory Animals, the Association for Research in Vision and Ophthalmology Statement for the Use of Animals in Ophthalmic and Vision Research, and Institutional Animal and Care Use Committees of both the Wayne State University and the University of Florida. Animals were housed and maintained in 12-hour:12-hour light-dark cycle laboratory lighting, unless otherwise noted.

Groups

The following mix of male and female mice, all on a C57Bl/6 background, were studied: wild-type adult mice (2–3 mo. of age) or P7 mice (Jackson Laboratories, Bar Harbor, ME), and adult *Gnat1*$^{-/-}$ mice (kind gift of Dr Janis Lem). The RPE-specific MnSOD knockout mice (2–3 months of age) were generated as previously described after seven generations of breeding with C57Bl/6 wild-type mice.[24] Briefly, experimental mice in which exon 3 of *Sod2* was flanked by *loxP* sites were also transgenic for P_{VMD2}-*rtTA* and *tetO-*P_{hCMV} *cre*, so that cre recombinase was expressed only in the RPE. Pups of this genotype (*Sod2*$^{flox/flox}$*VMD2cre*) were induced to express cre recombinase by feeding doxycycline-laced chow to nursing dams for 2 weeks after delivery (P1–P14).[24] Two control groups were used: (1) doxycycline-treated *Sod2*$^{flox/flox}$ mice lacking the cre transgene and (2) C57Bl/6 wild-type mice (2–3 months of age). Magnetic resonance imaging examination occurred 6 to 8 weeks after cessation of doxycycline treatment.

Dark-adapted RPE-specific MnSOD knockout mice were studied either untreated, or with pretreatment by a combination of two antioxidants, methylene blue (MB, an alternate electron transporter that effectively inhibits superoxide generation by mitochondria), and α-lipoic acid (LPA, a potent free radical scavenger).[9,21,28,29] Approximately 24 hours before MRI examination, mice were injected with 1 mg/kg MB (dissolved in saline) intraperitoneally (IP). The next day, approximately 1 hour before the MRI examination, each MB-treated mouse was also treated with 50 mg/kg LPA (dissolved in saline and pH adjusted to ~7.4) IP.

Magnetic Resonance Imaging

The general mouse preparation for high resolution MRI is well established in our laboratory.[13,21] All animals were maintained in darkness for at least 16 hours before and during the dark phase of the MRI examination. In all groups, immediately before the MRI experiment, animals were anesthetized with urethane (36% depth solution IP; 0.083 mL/20 g animal weight, prepared fresh daily; Sigma-Aldrich Corp., St. Louis, MO, USA). Adults were treated topically with 1% atropine to ensure dilation of the iris during light exposure followed by 3.5% lidocaine gel to reduce sensation that might trigger eye motion, and to keep the ocular surface moist. P7 mice did not undergo a canthotomy, but we have previously shown that ~300 lux room light is sufficient to activate retinal melanopsin in vivo.[30] In all cases, high resolution 1/T1 data (details below) were acquired on a 7 T system (ClinScan; Bruker Corporation, Billerica, MA, USA) using a receive-only surface coil (1.0 cm diameter) centered on the left eye. Each 1/T1 data set takes 15 minutes to collect. 1/T1 data were collected first in the dark and then at 13 minutes and 29 minutes (midpoint of acquisition) after turning on the light. Unfortunately, our current data acquisition time ability precludes examination of 1/T1 responses at earlier time points. The end of a fiber optic bundle was attached to a light source (Mark II Light Source; Prescott's, Inc., Monument, CO, USA) placed caudal to the eye, projecting onto a white screen ~1 cm from eye, similar to that previously described.[31] We exposed the eye to 0 (i.e., dark) or ~530 lux (confirmed outside the magnet before and after each MRI run using a Traceable Dual-Range Light Meter (Control Company, Friendswood, TX, USA) placed against a 1-cm diameter aperture; measured this way, room lighting is ~300 lux). In all cases, animals were humanely euthanized as detailed in our Division of Laboratory Animal Resources (DLAR)-approved protocol.

The 1/T1 MRI procedure has been described in detail previously.[13,21] Retinal partial saturation T_1 data were acquired using a dual coil mode on a 7 T Bruker ClinScan system: Several single spin-echo (time to echo [TE] 13 ms, 7×7 mm^2, matrix size 160×320, slice thickness 600 μm, in-plane resolution 21.9 μm) images were acquired at different repetition times (TRs) in the following order (number of images collected per time between repetitions in parentheses): TR 0.15 seconds (6), 3.50 seconds (1), 1.00 seconds (2), 1.90 seconds (1), 0.35 seconds (4), 2.70 seconds (1), 0.25 seconds (5), and 0.50 seconds (3). In other words, to compensate for reduced signal to noise ratios at shorter TRs, progressively more images were collected as the TR decreased. During an MRI session, animals were studied in an alternating order between controls and experimental mice.

MRI Data Analysis

In each adult animal, we confirmed ocular dilation based on the iris position on the MRI data.[32] 1/T1 MRI data from the central retinal (±1 mm from the center of the optic nerve) were analyzed as previously described.[13] Single images acquired with the same TR were first registered (rigid body) and then averaged. These averaged images were then co-registered across TRs. The central retinal regions-of-interest were analyzed by calculating 1/T1 maps by fitting to a three-parameter T1 equation ($y = a + b^*(\exp(-c^*TR))$, where a, b, and c are fitted parameters) on a pixel-by-pixel basis using R (version 2.9.0; R Development Core Team, Vienna, Austria) scripts developed in-house, and the minpack.lm package (version 1.1.1, Timur V. Elzhov and Katharine M. Mullen minpack.lm: R interface to the Levenberg-Marquardt nonlinear least-squares algorithm found in MINPACK. R package version 1.1–1). The reciprocal ($1/T_1$) values directly reflect paramagnetic free radical levels.[21,33] Central intraretinal $1/T_1$ profiles were obtained as detailed elsewhere.[32] Transretinal profiles from the superior and inferior retina were averaged.

As in our previous study, day-to-day variability was minimized in the MRI experiments by collecting data from at least three control mice studied alternatively with at least three experimental mice.[21] Correction factors were calculated at each retinal depth to adjust the mean control 1/T1 values of the same-day controls to a reference set of control 1/T1 values.[21] These depth-specific correction factors were then

Investigative Ophthalmology & Visual Science

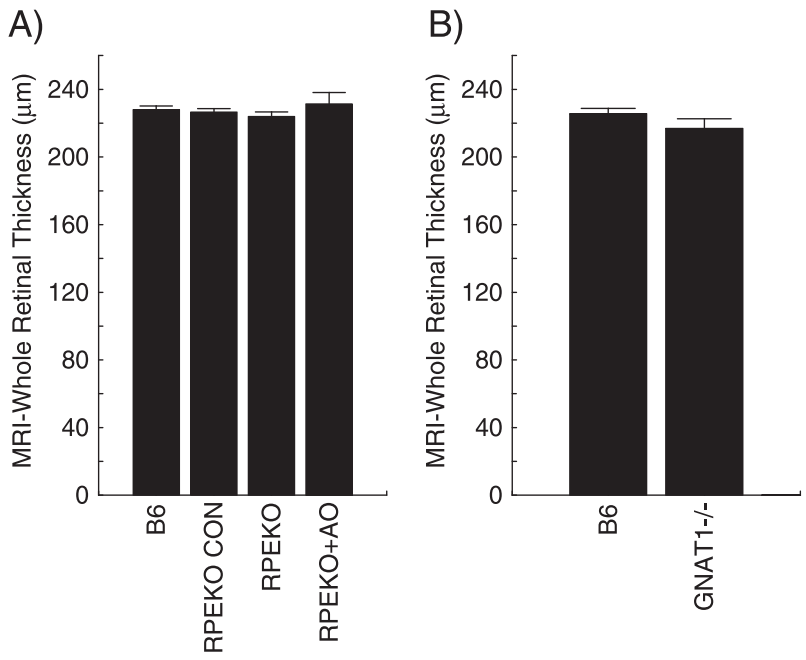

Figure 1. Magnetic resonance imaging-based whole retinal thickness summary. Comparison of dark-adapted thickness in (**A**) wild-type mice ("B6," $n = 20$), doxycycline-treated *Sod2*$^{flox/flox}$ mice lacking the cre transgene ("RPEKO controls," $n = 7$), doxycycline-treated *Sod2*$^{flox/flox}$ mice expressing cre recombinase ("RPEKO," $n = 5$), and RPEKO mice treated with antioxidant (AO) ("RPEKO+AO," $n = 5$), and (**B**) wild-type mice ("B6," $n = 10$) and *Gnat1*$^{-/-}$ mice ($n = 5$). No significant differences across any groups in (**A**) or (**B**) were noted. Error bars represent SEM.

applied to the experimental data from that day; the Y-axis is labeled as "Adjusted 1/T1." Because P7 mice data were not collected in this fashion, their Y-axis represents 1/T1 and their data are presented on a separate graph.

In each mouse, retinal thicknesses (μm) were objectively determined from MRI data using the "half-height method" wherein a border is determined via a computer algorithm based on the crossing point at the midpoint between the local minimum and maximum, as detailed elsewhere.[32,34] The distance between two neighboring crossing-points thus represents an objectively defined thickness. Thickness values were then normalized with 0% depth at the presumptive vitreoretinal border and 100% depth at the presumptive retina-choroid border. As previously discussed, the dark-to-light transition produces a significant increase in choroidal but not retinal thickness.[35–37] To minimize the impact of the light-evoked choroidal expansion on the present analysis, and to allow for comparisons between groups and conditions, 1/T1 transretinal profiles in dark and light in each mouse were spatially normalized to the anatomical thickness value in the dark.[38]

Spectral-Domain OCT (SD-OCT)

One wild-type mouse and one RPE-specific MnSOD knockout mouse treated with antioxidants were randomly chosen for OCT examination (Envisu R2200 VHR SDOIS System; Bioptigen, Inc., Durham, NC, USA). Mice were anesthetized with ketamine and xylazine for the examination. Optical coherence tomography was not performed in the *Gnat1*$^{-/-}$ group because (1) the MRI retinal thickness measurements are not significantly different from that in the wild-type mice (Fig. 1),[25,39] and (2) with only five mutant mice available to be examined by MRI, we did not want to risk possible anesthetic deaths. Instead, OCT measurements of wild-type mice were used in the 1/T1 transretinal profile of *Gnat1*$^{-/-}$ mice because of a previous report that mice lacking *Gnat1* and arrestin1 had nearly normal laminar structure.[40] Optical coherence tomography was also not performed in P7 mice because they did not have a clear optical path due to closed eyelids and the presence of an intact hyaloidal circulation.[30]

Statistical Analysis

As in our previous studies, promising MRI transretinal profile location ranges of significant differences were initially suggested using a one-tailed unpaired *t*-test at different locations of the adjusted 1/T1 transretinal profiles; for these "unofficial" comparisons, no tests for normality of data were performed.[38,39,41,42] If the *t*-test suggested significance ($P \leq 0.05$) over a select location range, a more formal statistical analysis using a generalized estimating equation (GEE) approach was used.[38,39,41–43] The GEE method is a more powerful two-tailed method that performs a general linear regression analysis using contiguous locations in each subject and accounts for the within-subject correlation between contiguous locations even if the normality assumption is not validated.[43,44] Differences on GEE analysis were considered statistically significant at $P < 0.05$. Data are presented as mean ± standard error of the mean (SEM).

Results

Elevated 1/T1 Values in RPE-Specific MnSOD Knockout Mice

Dark-adapted RPE-specific MnSOD knockout mice had greater ($P < 0.05$) 1/T1 values in all layers of the outer retina than the doxycycline-treated *Sod2*$^{flox/flox}$ mice lacking the cre transgene control group (Fig. 2A), and supernormal 1/T1 levels in the RPE, outer segments, and outer nuclear layers compared to the wild-type control mice (Fig. 2B). MB+LPA treatment significantly ($P < 0.05$) corrected these supernormal values to levels of both control groups, indicating that the outer retinal

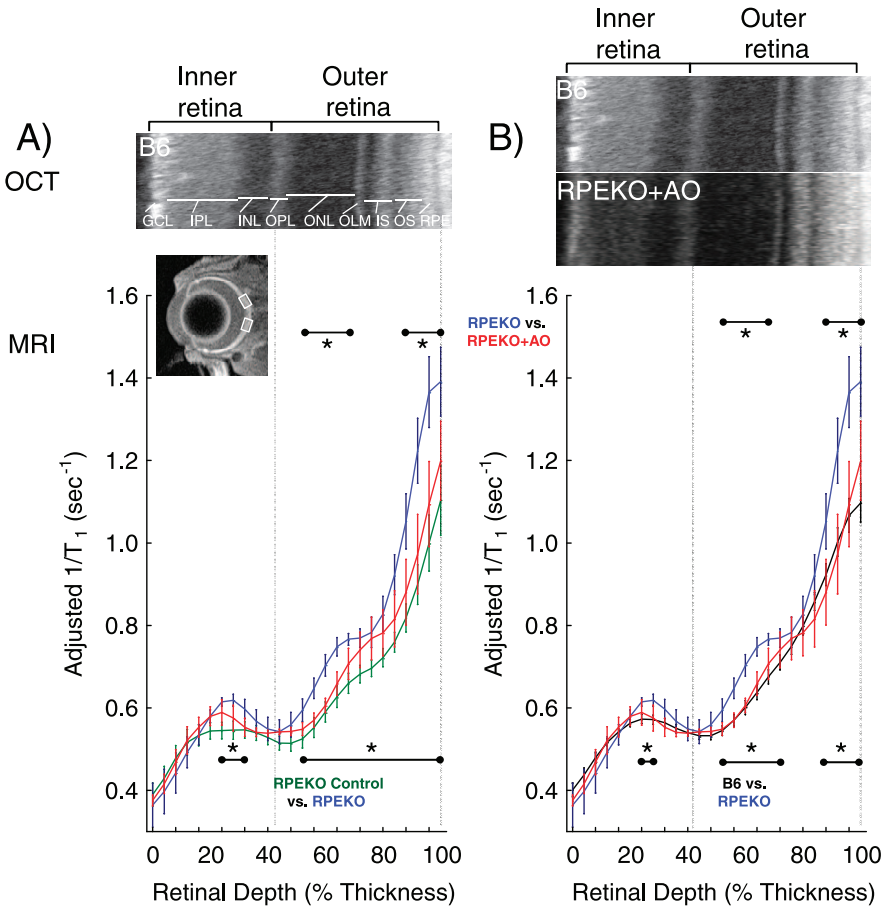

Figure 2. Quench-assisted MRI measurement in vivo of outer retina oxidative stress. (**A**) 1/T1 MRI profiles in vivo comparing one dark-adapted control group, doxycycline-treated *Sod2*$^{flox/flox}$ mice lacking the cre transgene ("RPEKO controls," *green, n* = 7), doxycycline-treated *Sod2*$^{flox/flox}$ mice expressing cre recombinase ("RPEKO," *blue*, *n* = 5), and RPEKO mice treated with antioxidant (AO) ("RPEKO+AO," *red*, *n* = 5). (**B**) 1/T1 MRI profiles in vivo comparing another dark-adapted control group, wild-type mice ("B6," *black*, *n* = 20), doxycycline-treated *Sod2*$^{flox/flox}$ mice expressing cre recombinase ("RPEKO," *blue*, *n* = 5), and RPEKO mice treated with AO ("RPEKO+AO," *red*, *n* = 5). In both graphs, representative OCT images (*above*) illustrate laminar spacing within the retina; layer assignments are presented.[66] *Dashed vertical lines* map outer plexiform layer (OPL) (42%) and retina/choroid boundary (100%) onto MRI profiles (*below*); MRI insert shows regions studied (*white boxes*); visual inspection of each groups' MRI does not allow for easy appreciation of differences in the derived parameter 1/T1 and so only a representative image is presented. *Retinal depth range with significant difference ($P < 0.05$). Adjusted 1/T1 data at each depth used factors that normalize same-day B6 controls to a B6 control reference data set. GCL, ganglion cell layer; INL, inner nuclear layer; IPL, inner plexiform layer; IS, rod inner segment layer; OLM, outer limiting membrane; ONL, outer nuclear layer; OPL, outer plexiform layer; OS, rod outer segment layer.

supernormal 1/T1 values resulted from excessive free radical production. Inner retina had a small but still significant elevation in 1/T1 ($P < 0.05$) over control values that were not correctable by antioxidant treatment suggesting either a non–free radical etiology or lack of detection sensitivity. Comparing the two control groups revealed a significant decrease in 1/T1 ($P < 0.05$) in the outer retina (76%–92% depth, data not shown); more work is needed to clarify this difference. The retina's laminar architecture was normal on visual inspection of a representative OCT image (Fig. 2B); quantitatively, whole retinal thickness MRI measurements in all groups were unremarkable (Fig. 1A).

Light Evoked Reduction of 1/T1 in Adult Wild-Type Mice

As shown in Figure 3A, adult C57Bl/6 wild-type mice demonstrated in vivo light-evoked reductions ($P < 0.05$) in 1/T1 of rod cells, compared to that in the dark. By 13 minutes of light, 1/T1 was significantly ($P < 0.05$) reduced at 80% to 100% depth into the retina (i.e., the presumptive ellipsoid and outer segment regions that contain ~75% of the retina's mitochondria[45]); by 29 minutes of light significant ($P < 0.05$) reduction of 1/T1 was evident over a larger extent of outer retina (60%–100% depth) including the presumptive outer nuclear layer. In addition, 13 minutes of light lowered ($P < 0.05$) 1/T1 significantly at 28% to 40% depth, which corresponded to the inner nuclear layer on OCT. This change was not observed ($P > 0.05$) by 29 minutes of light. These results were not related to duration of anesthetic because, as noted previously, prolonging the duration of dark did not decrease outer retinal 1/T1 values (data not shown).[21]

Light Evoked Reduction of 1/T1 in *Gnat1*$^{-/-}$ Mice

In dark-adapted *Gnat1*$^{-/-}$ mice, unlike in wild-type mice, light reduced ($P < 0.05$) outer retinal 1/T1 to similar extents by 13 minutes (64%–100% depth) and 29 minutes (60%–100% depth) (Fig. 3B). In addition, outer retina-specific 1/T1 values were visually higher than that of wild-type mice regardless of dark or light adaptation. Light produced an increase ($P < 0.05$) in inner retina 1/T1 by 13 (0%–12% depth) and 29 minutes (0%–16% depth) (Fig. 3B). Whole retinal thickness values on MRI

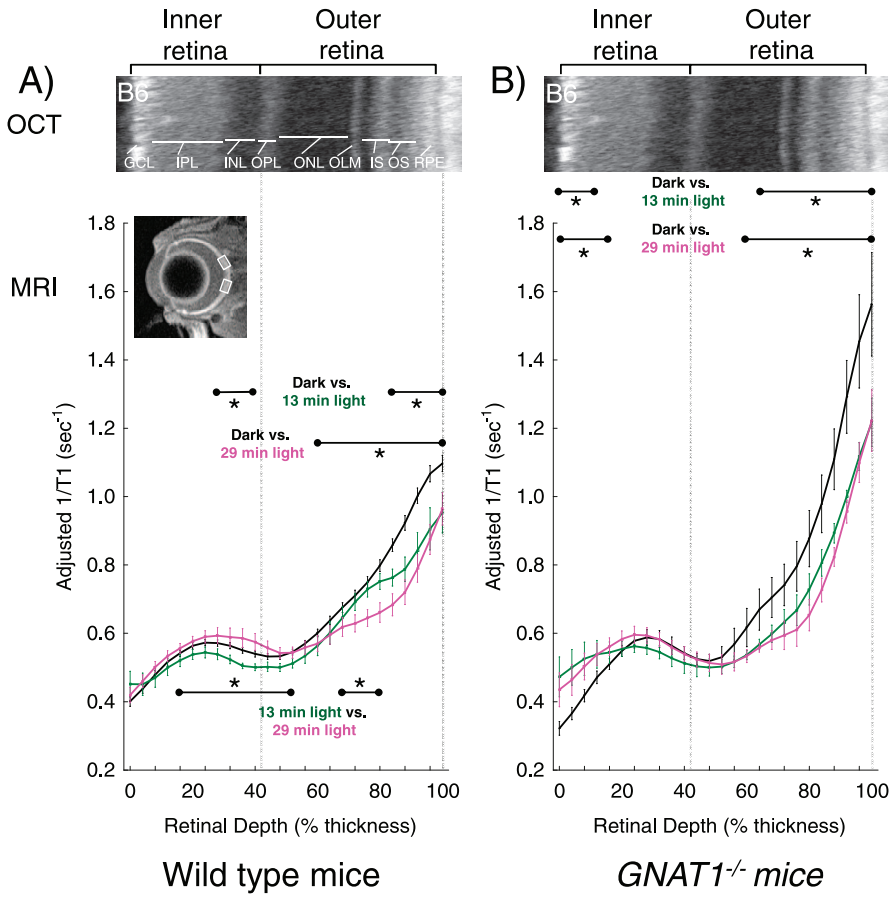

Figure 3. Light quench-assisted MRI measurement in adult mice in vivo. 1/T1 MRI profiles from (**A**) C57Bl/6 mice ($n = 7$) and (**B**) *Gnat1*$^{-/-}$ mice ($n = 5$) exposed in a paired-fashion to dark (*black symbols*) then light inside the magnet for 13 minutes (*green symbols*) and 29 minutes (*pink symbols*). Graphing conventions are as in Figure 2.

examination were not different ($P > 0.05$) between wild-type and *Gnat1*$^{-/-}$ mice (Fig. 1B).

P7 Wild-Type Mice

In contrast to the light-evoked outer retina changes observed in adult mice, P7 mice (which have active inner, but not outer, retinal photosensitivity[30]) did not demonstrate any light-dependent changes in inner or outer retina 1/T1 values ($P > 0.05$) (Fig. 4). While the data collection protocol for the P7 mice prevented direct quantitative comparisons with adult wild type data, visual inspection suggests that the maximum 1/T1 transretinal value was lower than that in wild-type adults and the overall shape of the transretinal 1/T1 profile was flatter than in the adult (see Methods section). As expected, whole retinal thickness values were different ($P < 0.05$) between adult wild-type mice (225 ± 3 μm; $n = 10$) and P7 mice (254 ± 6 μm; $n = 4$).[30]

Discussion

Here, we take advantage of nearly a decade of research by our lab and others validating MRI's ability to resolve differences in function between different retinal layers in vivo based on 1/T1 (and other MRI contrast mechanisms); retinal-layer assignments are supported by aligning transretinal functional MRI profiles against representative OCT images.[21,46] The present results support our previous suggestion that quench-assisted MRI is a reliable readout in vivo of total free radical burden in the outer retina.[21] Quench-assisted MRI changes in the inner retina are currently more challenging to interpret because they may represent (1) a direct change in free radical production, (2) an indirect downstream neuronal effect linked with changes in the outer retina, and/or (3) be influenced by hemodynamic-linked factors since the inner retina is vascularized.

It is important to consider whether or not quench-assisted MRI could reflect functional changes in factors other than free radicals, such as pO_2, pH, or hemodynamics. For example, it is well established that light increases pO_2 of rod cells (compared to that in the dark).[23,47] However, if paramagnetic oxygen were the dominant 1/T1 contrast mechanism measured herein,[48,49] the known increase in pO_2 in the outer retina with light would increase 1/T1, but instead rod cell 1/T1 decreases in the light consistent with reduced mitochondrial activity.[23,47] In addition, 1/T1 per se is not particularly sensitive to pH in vivo.[50] A hemodynamic etiology is unlikely because the outer retina is avascular. Free radicals thus represent the most cogent mechanism for understanding quench-assisted MRI results in all conditions studied to-date.[21]

Quench-Assisted MRI of Outer Retinal Oxidative Stress In Vivo

In our previous study, systemic injection of low dose sodium iodate was used to produce oxidative stress in RPE and rod layers, based on previous results obtained ex vivo.[21] Quench-assisted MRI indeed measured in vivo oxidative stress only in the outer retina.[21] In this study, we examined the RPE-specific

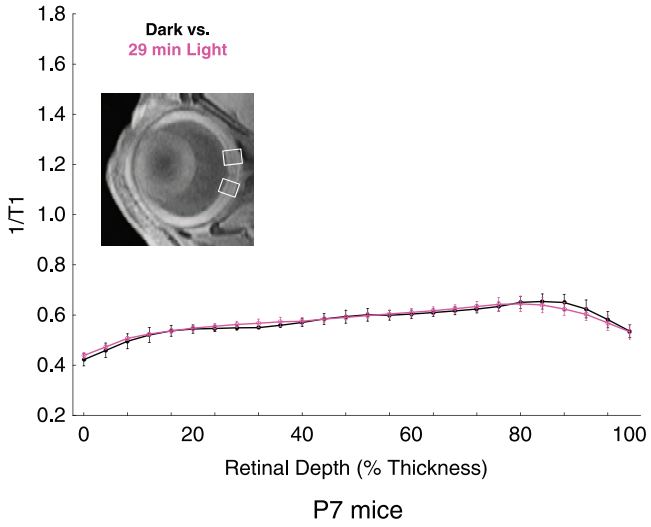

FIGURE 4. Quench-assisted MRI measurement in P7 C57Bl/6 mice in vivo. 1/T1 MRI profiles from P7 mice ($n = 4$) exposed in a paired-fashion to dark (*black symbols*) then light inside the magnet for 29 minutes (*pink symbols*). Graphing conventions are as in Figure 2. Optical coherence tomography is not presented because at P7 mice lack a clear optical path due to closed eyelids and the presence of an intact hyaloidal circulation.[30]

MnSOD knockout mouse, a nonpharmacologic model thought to specifically produce oxidative stress in RPE.[24] We examined two controls for this mutant mouse: doxycycline-treated *Sod2*$^{flox/flox}$ mice lacking the cre transgene on a C57Bl/6 background and C57Bl/6 wild-type controls. Retinal pigment epithelium-specific MnSOD knockout mice had a quenchable, supernormal 1/T1 signal in the RPE indicative of oxidative stress. Somewhat surprisingly, the presumptive outer nuclear layer of these mice also showed evidence of oxidative stress; this will be a topic of future investigation.

Gnat1$^{-/-}$ mice demonstrated retinal oxidative stress based on previous data from a lucigenin superoxide assay ex vivo.[51] Here, we observe a greater than normal 1/T1 in the outer retina in both dark and light adapted *Gnat1*$^{-/-}$ mice consistent with the presence of oxidative stress. The mechanism causing oxidative stress in *Gnat1*$^{-/-}$ mice is unclear and not the focus of this study. However, we speculate that the oxidative stress in *Gnat1*$^{-/-}$ mice in the light may result, at least in part, from the reported build-up of *bis*-retinoids, which can generate excessive free radical production upon photoactivation.[27,52] In any event, these data support the spatial and detection sensitivity of quench-assisted MRI to outer retinal oxidative stress.

Strain Sensitivity of Light Quench-Assisted MRI In Vivo

Previously, we found that rod dominant 129S6 adult wild-type mice evaluated at 29 minutes of light had rod cell 1/T1 that was reduced at 84% to 100% depth into the retina, compared to that in the dark.[21] In the present study we examined another common mouse strain, the C57Bl/6 mice at two time points of light exposure. In the C57Bl/6 mice, light reduced outer retinal 1/T1 but with a different spatiotemporal profile than that of 129S6 mice. In particular, in C57Bl/6 mice, the spatial extent of 1/T1 reduction by 13 minutes of light exposure (80%–100% depth) was similar to that after 29 minutes of light (the only time point studied in 129S6 mice) in 129S6 mice (84%–100% depth). By 29 minutes of light, neither strain showed inner retinal changes in 1/T1. Together, the above considerations suggest that light quench-assisted MRI is sensitive to strain differences in spatiotemporal rod cell responses to light.

Genetic background is well known to substantially influence mouse physiology and pathophysiology.[53–55] C57Bl/6 and 129S6 (the wild-type strain studied by quench-assisted 1/T1 MRI previously[21]) mice exhibit differences in cone-based photopic optokinetic responses.[56] To the best of our knowledge, differences in rod cell biology between C57Bl/6 and 129S6 mice strains have not been studied. Different isoforms of RPE65 have been identified in C57Bl/6 (with its Met450 isoform leading to relatively slow pigment regeneration in the light) and 129S6 (with its Leu450 isoform resulting in relatively fast pigment regeneration) mice.[57] Our previous data found that very fast pigment regeneration in cones was associated with similar outer retinal 1/T1 in dark and light.[21] Thus, one explanation for the different light-stimulated spatiotemporal profiles in the outer retina of C57Bl/6 and 129S6 may be that rods with faster pigment regeneration (e.g., the 129S6 mice) will produce adenosine triphosphate (ATP) at a faster rate and thus have relatively greater production of free radical production in the light resulting in a smaller dark/light difference in outer retina 1/T1 than rods with slower pigment regeneration (e.g., the C57Bl/6 mice).[23,58] These considerations suggest that the speed of pigment regeneration via the visual cycle is a contributing factor to the kinetics of light quench-assisted MRI results in outer retina in vivo.

Light Quench-Assisted MRI of Immature Retina In Vivo

In this study, light quench-assisted MRI was also used to confirm the hypothesis that developing and photo-insensitive rod outer segments at P7 will show similar outer retinal 1/T1 values in dark and light.[30,59–61] The 1/T1 profile at P7 (Fig. 4) appears relatively flat compared to the adult profile (e.g., Fig. 3A) suggesting little intraretinal differences between inner and outer retina in continuous production of free radicals during development also consistent with immature outer retina.[30,59–61] Interestingly, by P7 inner retina intrinsically photosensitive retinal ganglion cells (ipRGCs) are mature enough to detect light, even in the presence of fused eyelids, a tunica vasculosa lentis, and a hyaloid circulation.[30] However, no light induced reduction in 1/T1 in the inner retina was measured with light quench-assisted MRI (Fig. 4). We speculate that this is at least in part due to a 10^4-fold lower membrane melanopsin density, compared to that of rod pigment, resulting in a relatively lower photo-catch.[62] The lack of light induced free radical quench in the outer retina of the P7 mouse model provides good negative control data that supports light quench-assisted MRI sensitivity to outer retina phototransduction and visual cycle activity.[63] These results set the stage for a more detailed future developmental study that compares, at different levels of maturity, light quench-assisted MRI outcomes to ERG metrics, MRI measures of rod function, and optokinetic tracking data.

Light Quench-Assisted MRI in the Absence of an Essential Component of Traditional Rod Phototransduction In Vivo

Gnat1$^{-/-}$ mice demonstrated a large and robust light suppression of 1/T1 in the outer retina relative to that in the dark with a faster spatiotemporal pattern than in wild-type C57Bl/6 mice (Fig. 3). Although *Gnat1*$^{-/-}$ mice have fully functional cone photoreceptors, these do not seem to be contributing to the *Gnat1*$^{-/-}$ mice light response for the following reasons.[25,26,39] First, as shown in our previous study of cone-only *R91W;Nrl*$^{-/-}$ mice, light does not change outer retinal 1/T1 values in the

dark and light, consistent with the fact that cones do not saturate in the light.[21] Second, the response of 1/T1 in the outer retina to light in *Gnat1*$^{-/-}$ mice most resembled that in rod-dominated mouse retina and not that from *R91W;Nrl*$^{-/-}$ cone-only mice. Third, numerically, cones comprise only ~3% depth of photoreceptors in mice with a C57Bl/6 background.[64]

Gnat1$^{-/-}$ mice experience normal rhodopsin bleaching and this will lead to an increase in the production of ATP (and thus a presumed increase in mitochondrial leakage of free radicals) for the visual cycle.[23] In wild-type mice, light reduces rod free radicals produced by the maintenance of the dark current, but will also trigger an increase in free radicals due to visual cycle activation.[23] Thus, opposing mechanisms modify the net production of free radicals when turning on the light. These opposing mechanisms likely strike a different balance in rods from wild-type and *Gnat1*$^{-/-}$ mice, but more work is needed to unravel exact mechanisms.

Summary

This study provides additional evidence to support the use of quench-assisted MRI to close the technology gap in measuring outer retinal free radical production in vivo.[21] We anticipate that light quench-assisted MRI will be translatable to humans in the near future, based on recent high resolution MRI of the human retina obtained without sedation using a cued-blinking procedure.[65] In addition, because of the specific topography of human retinas, the contribution of cones will have to be studied in more detail using quench-assisted MRI, such as their sensitivity to ultraviolet illumination, in addition to light related rod, cone, and RPE processes presented here and elsewhere.[21]

Acknowledgments

We thank Vladimir Kefalov (Washington University in St. Louis) and Janis Lem (Tufts University) for their helpful conversations.

Supported by the National Institutes of Health (NIH) Grant EY021619 (BAB), NIH EY020825 (ASL), P30-EY021721 (ASL), the Macula Vision Research Foundation (ASL), and an unrestricted grant from Research to Prevent Blindness (BAB).

Disclosure: **B.A. Berkowitz**, None; **A.S. Lewin**, None; **M.R. Biswal**, None; **B.X. Bredell**, None; **C. Davis**, None; **R. Roberts**, None

References

1. Rohrer B, Pinto FR, Hulse KE, Lohr HR, Zhang L, Almeida JS. Multidestructive pathways triggered in photoreceptor cell death of the RD mouse as determined through gene expression profiling. *J Biol Chem*. 2004;279:41903–41910.
2. Fukuda S, Ohneda O, Oshika T. Oxidative stress retards vascular development before neural degeneration occurs in retinal degeneration rd1 mice. *Graefes Arch Clin Exp Ophthalmol*. 2014;252:411–416.
3. Yang LP, Wu LM, Guo XJ, Tso MO. Activation of endoplasmic reticulum stress in degenerating photoreceptors of the rd1 mouse. *Invest Ophthalmol Vis Sci*. 2007;48:5191–5198.
4. Sanz MM, Johnson LE, Ahuja S, Ekstrom PA, Romero J, van VT. Significant photoreceptor rescue by treatment with a combination of antioxidants in an animal model for retinal degeneration. *Neuroscience*. 2007;145:1120–1129.
5. Jaliffa C, Ameqrane I, Dansault A, et al. Sirt1 involvement in rd10 mouse retinal degeneration. *Invest Ophthalmol Vis Sci*. 2009;50:3562–3572.
6. Usui S, Komeima K, Lee SY, et al. Increased expression of catalase and superoxide dismutase 2 reduces cone cell death in retinitis pigmentosa. *Mol Ther*. 2009;17:778–786.
7. Komeima K, Rogers BS, Lu L, Campochiaro PA. Antioxidants reduce cone cell death in a model of retinitis pigmentosa. *PNAS*. 2006;103:11300–11305.
8. Du Y, Cramer M, Lee CA, et al. Adrenergic and serotonin receptors affect retinal superoxide generation in diabetic mice: relationship to capillary degeneration and permeability. *FASEB J*. 2015;29:2194–204.
9. Du Y, Veenstra A, Palczewski K, Kern TS. Photoreceptor cells are major contributors to diabetes-induced oxidative stress and local inflammation in the retina. *PNAS*. 2013;110:16586–16591.
10. Campochiaro PA, Strauss RW, Lu L, et al. Is there excess oxidative stress and damage in eyes of patients with retinitis pigmentosa? *Antioxid Redox Signal*. 2015;123:643–648.
11. Galbinur T, Obolensky A, Berenshtein E, et al. Effect of para-aminobenzoic acid on the course of retinal degeneration in the rd10 mouse. *J Ocul Pharmacol Ther*. 2009;25:475–482.
12. Zeng H, Ding M, Chen XX, Lu Q. Microglial NADPH oxidase activation mediates rod cell death in the retinal degeneration in rd mice. *Neuroscience*. 2014;275:54–61.
13. Berkowitz BA, Bissig D, Patel P, Bhatia A, Roberts R. Acute systemic 11-cis-retinal intervention improves abnormal outer retinal ion channel closure in diabetic mice. *Mol Vis*. 2012;18:372–376.
14. Berkowitz BA, Gradianu M, Bissig D, Kern TS, Roberts R. Retinal ion regulation in a mouse model of diabetic retinopathy: natural history and the effect of Cu/Zn superoxide dismutase overexpression. *Invest Ophthalmol Vis Sci*. 2009;50:2351–2358.
15. Zheng L, Du Y, Miller C, et al. Critical role of inducible nitric oxide synthase in degeneration of retinal capillaries in mice with streptozotocin-induced diabetes. *Diabetologia*. 2007;50:1987–1996.
16. Berkowitz BA, Roberts R, Stemmler A, Luan H, Gradianu M. Impaired apparent ion demand in experimental diabetic retinopathy: correction by lipoic acid. *Invest Ophthalmol Vis Sci*. 2007;48:4753–4758.
17. Prunty MC, Aung MH, Hanif AM, et al. In vivo imaging of retinal oxidative stress using a reactive oxygen species-activated fluorescent probe. *Invest Ophthalmol Vis Sci*. 2015;56:5862–5870.
18. Ekanger LA, Allen MJ. Overcoming the concentration-dependence of responsive probes for magnetic resonance imaging. *Metallomics*. 2015;7:405–421.
19. Zhelev Z, Bakalova R, Aoki I, Lazarova D, Saga T. Imaging of superoxide generation in the dopaminergic area of the brain in Parkinson's disease, using mito-TEMPO. *ACS Chem Neurosci*. 2013;4:1439–1445.
20. Rayner CL, Bottle SE, Gole GA, Ward MS, Barnett NL. Real-time quantification of oxidative stress and the protective effect of nitroxide antioxidants. *Neurochem Int*. 2016;92:1–12.
21. Berkowitz BA, Bredell BX, Davis C, Samardzija M, Grimm C, Roberts R. Measuring in vivo free radical production by the outer retina. *Invest Ophthalmol Vis Sci*. 2015;56:7931–7938.
22. Stinnett G, Moore K, Samuel E, et al. A novel assay for the in vivo detection of reactive oxygen species using MRI. *ISMRM Meeting Abstracts*. 2015;1917.
23. Okawa H, Sampath AP, Laughlin SB, Fain GL. ATP consumption by mammalian rod photoreceptors in darkness and in light. *Curr Biol*. 2008;18:1917–1921.
24. Mao H, Seo SJ, Biswal MR, et al. Mitochondrial oxidative stress in the retinal pigment epithelium leads to localized retinal degeneration. *Invest Ophthalmol Vis Sci*. 2014;55:4613–4627.
25. Calvert PD, Krasnoperova NV, Lyubarsky AL, et al. Phototransduction in transgenic mice after targeted deletion of the

rod transducin alpha -subunit. *Proc Natl Acad Sci U S A*. 2000; 97:13913–13918.

26. Sakurai K, Chen J, Kefalov VJ. Role of guanylyl cyclase modulation in mouse cone phototransduction. *J Neurosci*. 2011;31:7991–8000.
27. Brill E, Malanson KM, Radu RA, et al. A novel form of transducin-dependent retinal degeneration: accelerated retinal degeneration in the absence of rod transducin. *Invest Ophthalmol Vis Sci*. 2007;48:5445–5453.
28. Wen Y, Li W, Poteet EC, et al. Alternative mitochondrial electron transfer as a novel strategy for neuroprotection. *J Biol Chem*. 2011;286:16504–16515.
29. Rouchette L, Ghibu S, Richard C, Zeller M, Cottin Y, Vergely C. Direct and indirect antioxidant properties of alpha -lipoic acid. *Mol Nutr Food Res*. 2013;57:114–125.
30. Berkowitz BA, Roberts R, Bissig D. Light-dependant intraretinal ion regulation by melanopsin in young awake and free moving mice evaluated with manganese-enhanced MRI. *Mol Vis*. 2010; 16:1776–1780.
31. Bissig D, Berkowitz BA. Light-dependent changes in outer retinal water diffusion in rats in vivo. *Mol Vis*. 2012;18:2561–2xxx.
32. Bissig D, Berkowitz BA. Same-session functional assessment of rat retina and brain with manganese-enhanced MRI. *NeuroImage*. 2011;58:749–760.
33. Vallet P, Van HY, Bonnet PA, Subra G, Chapat JP, Muller RN. Relaxivity enhancement of low molecular weight nitroxide stable free radicals: importance of structure and medium. *Magn Reson Med*. 1994;32:11–15.
34. Cheng H, Nair G, Walker TA, et al. Structural and functional MRI reveals multiple retinal layers. *Proc Natl Acad Sci U S A*. 2006;103:17525–17530.
35. Longo A, Geiser M, Riva CE. Subfoveal choroidal blood flow in response to light-dark exposure. *Invest Ophthalmol Vis Sci*. 2000;41:2678–2683.
36. Fuchsjäger-Mayrl G, Polska E, Malec M, Schmetterer L. Unilateral light-dark transitions affect choroidal blood flow in both eyes. *Vision Res*. 2001;41:2919–2924.
37. Fitzgerald ME, Gamlin PD, Zagvazdin Y, Reiner A. Central neural circuits for the light-mediated reflexive control of choroidal blood flow in the pigeon eye: a laser Doppler study. *Vis Neurosci*. 1996;13:655–669.
38. Berkowitz BA, Grady EM, Khetarpal N, Patel A, Roberts R. Oxidative stress and light-evoked responses of the posterior segment in a mouse model of diabetic retinopathy. *Invest Ophthalmol Vis Sci*. 2015;56:606–615.
39. Berkowitz BA, Grady EM, Roberts R. Confirming a prediction of the calcium hypothesis of photoreceptor aging in mice. *Neurobiol Aging*. 2014;35:1883–1891.
40. Levine ES, Zam A, Zhang P, et al. Rapid light-induced activation of retinal microglia in mice lacking Arrestin-1. *Vision Res*. 2014;102:71–79.
41. Giordano C, Roberts R, Krentz K, et al. Catalase therapy corrects oxidative stress-induced pathophysiology in incipient diabetic retinopathy. *Invest Ophthalmol Vis Sci*. 2015;56: 3095–3102.
42. Berkowitz BA, Murphy GG, Craft CM, Surmeier DJ, Roberts R. Genetic dissection of horizontal cell inhibitory signaling in mice in complete darkness in vivo. *Invest Ophthalmol Vis Sci*. 2015;56:3132–3139.
43. Liang Z. Longitudinal data analysis using generalized linear models. *Biometrika*. 1986;73:13–22.
44. Lu N, Tang W, He H, et al. On the impact of parametric assumptions and robust alternatives for longitudinal data analysis. *Biometr J Biometrische Zeitschrift*. 2009;51:627–643.
45. Perkins GA, Ellisman MH, Fox DA. Three-dimensional analysis of mouse rod and cone mitochondrial cristae architecture: bioenergetic and functional implications. *Mol Vis*. 2003;9:60–73.
46. Berkowitz BA, Bissig D, Roberts R. MRI of rod cell compartment-specific function in disease and treatment in vivo [published online ahead of print September 4, 2015]. *Prog Retin Eye Res*. doi:10.1016/j.preteyeres.2015.09.001.
47. Linsenmeier RA, Braun RD. Oxygen distribution and consumption in the cat retina during normoxia and hypoxemia. *J Gen Physiol*. 1992;99:177–197.
48. Berkowitz BA. Role of dissolved plasma oxygen in hyperoxia-induced contrast. *Magn Reson Imaging*. 1997;15:123–126.
49. Berkowitz BA. Adult and newborn rat inner retinal oxygenation during carbogen and 100% oxygen breathing. Comparison using magnetic resonance imaging delta Po2 mapping. *Invest Ophthalmol Vis Sci*. 1996;37:2089–2098.
50. Yamamoto F, Borgula GA, Steinberg RH. Effects of light and darkness on pH outside rod photoreceptors in the cat retina. *Exp Eye Res*. 1992;54:685–697.
51. Berkowitz BA, Wen X, Thoreson WB, Kern TS, Roberts R. Abnormal rod calcium homeostasis and the development of retinal oxidative stress in diabetes. *Invest Ophthalmol Vis Sci*. 2015;56:4280.
52. Sparrow JR, Zhou J, Ben-Shabat S, Vollmer H, Itagaki Y, Nakanishi K. Involvement of oxidative mechanisms in blue-light-induced damage to A2E-laden RPE. *Invest Ophthalmol Vis Sci*. 2002;43:1222–1227.
53. Walsh N, Bravo-Nuevo A, Geller S, Stone J. Resistance of photoreceptors in the C57BL/6-c2J, C57BL/6J, and BALB/cJ mouse strains to oxygen stress: evidence of an oxygen phenotype. *Curr Eye Res*. 2004;29:441–447.
54. Matsumoto H, Kataoka K, Tsoka P, Connor KM, Miller JW, Vavvas DG. Strain difference in photoreceptor cell death after retinal detachment in mice. *Invest Ophthalmol Vis Sci*. 2014; 55:4165–4174.
55. Crawley JN, Belknap JK, Collins A, et al. Behavioral phenotypes of inbred mouse strains: implications and recommendations for molecular studies. *Psychopharmacology (Berl)*. 1997;132:107–124.
56. Cahill H, Nathans J. The optokinetic reflex as a tool for quantitative analyses of nervous system function in mice: application to genetic and drug-induced variation. *PLoS ONE*. 2008;3:e2055.
57. Kolesnikov AV, Tang PH, Parker RO, Crouch RK, Kefalov VJ. The mammalian cone visual cycle promotes rapid M/L-cone pigment regeneration independently of the interphotoreceptor retinoid-binding protein. *J Neurosci*. 2011;31:7900–7909.
58. Falk G, Fatt P. Conductance changes produced by light in rod outer segments. *J Physiol*. 1968;198:647–699.
59. Ohki K, Yoshida K, Harada T, Takamura M, Matsuda H, Imaki J. C-fos gene expression in postnatal rat retinas with light/dark cycle. *Vis Res*. 1996;36:1883–1886.
60. Luo DG, Yau KW. Rod sensitivity of neonatal mouse and rat. *J Gen Physiol*. 2005;126:263–269.
61. Wetzel RK, Arystarkhova E, Sweadner KJ. Cellular and subcellular specification of Na,K-ATPase alpha and beta isoforms in the postnatal development of mouse retina. *J Neurosci*. 1999;19:9878–9889.
62. Do MT, Kang SH, Xue T, et al. Photon capture and signalling by melanopsin retinal ganglion cells. *Nature*. 2009;457:281–287.
63. Carter-Dawson L, Alvarez RA, Fong SL, Liou GI, Sperling HG, Bridges CDB. Rhodopsin, 11-cis vitamin A, and interstitial

Investigative Ophthalmology & Visual Science

retinol-binding protein (IRBP) during retinal development in normal and rd mutant mice. *Develop Biol*. 1986;116:431–438.

64. Carter-Dawson LD, Lavail MM, Sidman RL. Differential effect of the rd mutation on rods and cones in the mouse retina. *Invest Ophthalmol Vis Sci*. 1978;17:489–498.
65. Berkowitz BA, McDonald C, Ito Y, Tofts PS, Latif Z, Gross J. Measuring the human retinal oxygenation response to a hyperoxic challenge using MRI: eliminating blinking artifacts and demonstrating proof of concept. *Magn Reson Med*. 2001; 46:412–416.
66. Berger A, Cavallero S, Dominguez E, et al. Spectral-domain optical coherence tomography of the rodent eye: highlighting layers of the outer retina using signal averaging and comparison with histology. *PLoS ONE*. 2014;9:e96494.

Investigative Ophthalmology & Visual Science